Eco-friendly Method of Synthesis CeO₂ Nanoparticles by Watercress Plant Extract for Removal of Cibacron Red Dye from Aqueous Solutions

Aya Qasim Khanjar[1], Ahlam Mohammed Farhan[1], Ahmed Mahdi Rheima[2*]

[1] *Department of Chemistry, College of Sciences for Women, University of Baghdad Baghdad, Iraq*

[2] *Department of Chemistry, College of Science, Mustansiriyah University Baghdad, Iraq*

[*]*Corresponding Author:* ahmed.rheima@gmail.com

Abstract: Water dye contamination is a serious issue, particularly given that textile mills are the main cause. The development of medicines using nanomaterials has involved a lot of study and testing. This study discusses the environmentally friendly synthesis of CeO₂ nanoparticles using plant extract from watercress and calcination at 400°C for 3 hours. The SEM and TEM were used to examine nanoparticles, which were 36 nm. X-ray diffraction was utilized to determine the crystal structure. The purity of the synthetic material was confirmed by energy-dispersive X-ray spectroscopy (EDX) investigation of the structure of the produced product, which revealed just cerium (Ce) and oxygen (O) elements. The dye Cibacron red was more readily absorbed with the addition of CeO₂ NPs. The Cibacron red dye adhered to the CeO₂ nanoparticles more quickly after 30 minutes of contact. The best models for describing the adsorption process were those of Freundlich and pseudo-second-order with R₂ values greater than 0.9246 and 0.9873, respectively. Thermodynamic analysis was used to determine the parameters of 2.44 kJ/mol, 29.26 kJ/mol K, and 97.68 J/mol ΔG, ΔH, and ΔS. It can be concluded that the CeO₂ NPs function well as a Cibacron red dye adsorbate surface.

Key Words: CeO₂ nanoparticles (NPs)**,** adsorption, Cibacron red dye, green synthesis

1. Introduction

Environmental pollution is one of the main issues people nowadays have to deal with, and it becomes more dangerous due to numerous human activities. It has been discovered that environmental pollution is closely related to the global population growth [1]. One of the components that keeps life alive is water. Since millions of chemical compounds are discharged every day, directly or indirectly, to water sources without any treatment [2], freshwater supplies have recently seen a major decline as a result of technological advancement [3]. As a result, the issue of water contamination has attracted a lot of attention in the modern era [1]. Dyes are considered organic pollutants in aqueous systems and can pose a risk to all elements of the environment due to its toxicity, especially when they are present in high concentrations [4]. Dyes include all substances used to color textiles, leather, food, and other materials. Organic compounds are one of the most important components of industrial wastewater. There is a significant risk of long-term consequences since some organic pollutants have the potential to cause malignant diseases [5]. According to WHO reports, the bulk of diseases that spread in undeveloped countries are mostly caused by contaminated drinking water. Researchers have therefore used a variety of techniques to clean industrial water [6,7]. Diverse techniques have been used to cleanse and remove organic pol-lutants from industrial water. They comprise ion exchange, chemical oxidation, photo-oxidation, and the adsorption process, among others [8]. Adsorption is a method that is both efficient and affordable. Data from the WHO show that it is frequently used to clean up contaminated water [9-12]. Nanotechnology is used by many industries and sectors, such as the chemical industry, photoelectrochemical applications, environmental

health, medicine, and energy [13,14]. Nanotechnology [15], a crucial advancement in modern science, has made it possible to produce materials with distinctive size, structure, and substance. Production, processsing, and application all involve materials with a diameter less than a nanometer [16,17]. Physical, chemical, as well as biological characteristics at the nanoscale differ from bulk atoms and molecules individually [18-20]. This enables the creation of novel classes of cutting-edge chemicals and materials to satisfy the requirements of high-tech applications [21-24]. Cerium oxide (CeO_2), commonly referred to as nano ceria, is a superior semiconducting substance with a broad band gap energy of 3.19 eV, making it a strong choice for catalytic applications [25]. Due to their potential benefits in a number of applications, including a catalyst, an electrolyte material for solid oxide fuel cells, a diesel fuel additive, a material of high refractive index, an insulating layer on silicon substrates, gas sensors, and more recently biomedicine, significant efforts have been made in recent years to develop new synthetic methods for the preparation of nanostructure cerium oxides [26-30]. The biological impacts of nano ceria have been covered in numerous studies. It is well recognized that cerium oxide nanoparticles, in contrast to other metal oxide nanoparticles, do not have cytotoxic effects and instead offer protection against a variety of cellular damages, such as radiological shocks that encourage the generation of free radicals [31,32]. Cerium oxide nanoparticles have been created using a variety of tech-niques [33]. In this study, the green syn-thesis approach was used to make cerium oxide nanoparticles and used it to remove the Cibacron red dye, which is one of the dyes used in the textile industry in the Wasit

Governorate and most of which is disposed of as wastewater. The synthesis of nano-particles using plant extracts is a clean and safe method that does not contain harmful chemicals, but rather uses natural materials from plants.

2. Experimental

Extraction of the Watercress Plant Extract

Watercress plant extract has been collected and washed with deionized water to get rid of any dust. The dry leaves are gently blend-ed in a mixer to obtain homogeneous pow-ders. Then, 10 grams of leaves were ground and combined with 150 ml of deionized water. The mixture was then heated for 30 minutes at 60°C while being stirred. After filtering, the solution was placed in the refrigerator.

Synthesis of CeO₂ Nanoparticles

Cerium oxide nanoparticles were created using the green synthesis method. Accord-ingly, 400 ml of watercress filter had added to 0.01 mole of $Ce(NO_3)_3$ slowly (one drop every second) and stirred for 30 minutes. The yellow powder was repeatedly rinsed with deionized water, separated, and precip-itated. After being dried for an hour at 150°C, the precipitate was calcined for 3 hours at 400°C. The copper oxide nano-particles were produced as a yellowish white powder.

Cibacron Red Dye Adsorption on CeO₂ NPs

The equilibrium isotherm of a particular adsorbent serves as a representation of its adsorbent properties for the purpose of de-signing adsorption operations. A stock sol-ution of the Cibacron red dye (50 ppm) was made in deionized water. 0.01 g of CeO₂ nanoparticles were added to 10 ml of dye solution, and they were then heated to 298 K for 30 minutes. After the solution had been filtered, the dye concentration in the filtrate was measured using a UV-visible absorption spectrophotometer [34-35].

$$Qe = (C_{0\_} Ce)Vsol/M \qquad (1)$$

where Qe (mg/g) is the equilibrium adsorption capacity, C_0 and Ce are the beginning as well as equilibrium concen-trations of Cibacron red dye, and M is the mass of the CeO₂ nanoparticles (g). V sol is therefore the volume of Cibacron red (L).

Cerium Oxide Nanoparticles Characterization

X-ray diffraction was used to investigate the sample of CeO₂ nanoparticles (XRD-6000). The morphology of nanoparticles was studied using transmission electron microscopy. The shape of the CeO₂ nano-particles was studied under a scanning electron microscope (SEM). Nanoparticle morph-ology was examined using transmission electron microscopy (TEM).

3. Result and Discussion

The X-ray Diffraction of CeO₂ Nanoparticles

X-ray diffraction (XRD) in the 2θ range of 200-700 (Rigaku Miniflex II) utilizing Cu K radiations (λ = 1.54A) operated at a voltage of 30 kV and current of 15 mA was used to analyze the XRD pattern of cerium oxide nanoparticles displayed in Figure 1. The (111), (200), (220), (311), (222), and (400) cubic phase peaks are the diffracted peaks observed at diffraction angles 2θ of 28.270, 32.780, 47.050, 55.940, 59.070, and 69.090.
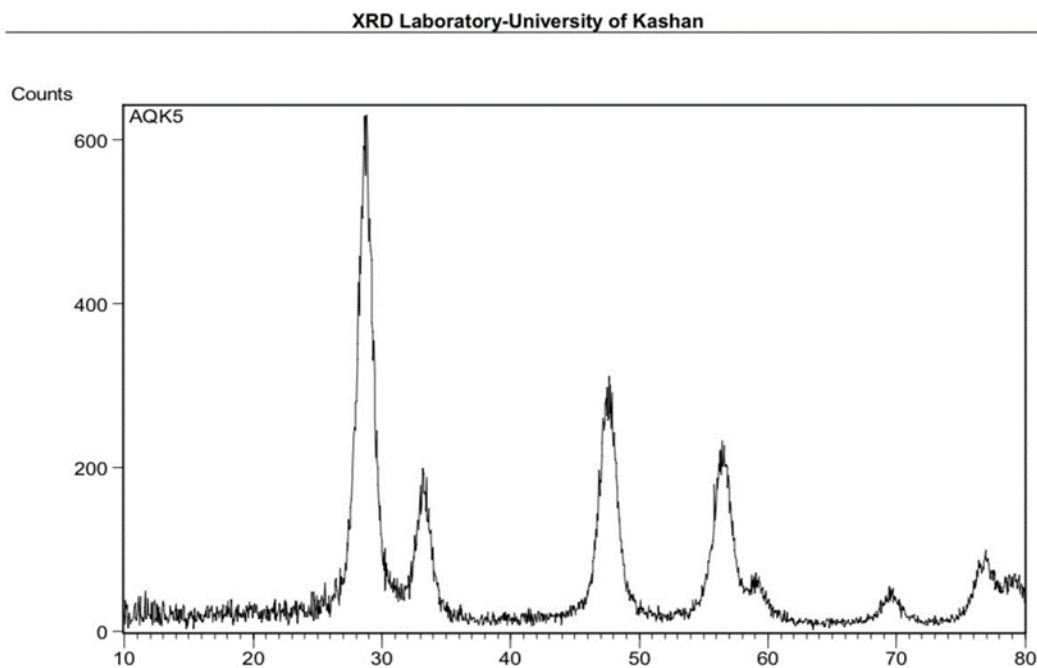

Figure 1. XRD Patterns of Cerium Oxide Nanoparticles

The spectra make it very evident that there are no additional contaminant peaks. Debye-Scherer equation [36] was used to calculate the crystallite size of cerium oxide nanoparticles, which was found to be 22 nm.

Field Emission Scanning Electron Microscope of CeO₂ Nanoparticles

FE-SEM was used to analyze the surface morphology of pure CeO₂ nanoparticles that had been calcined at 400°C. The SEM analysis revealed that the prepared sample was formed as spherical aggregates with a reasonably uniform distribution. Figure 2 displays the crystal nature of the equally-sized manufactured nanoparticles.
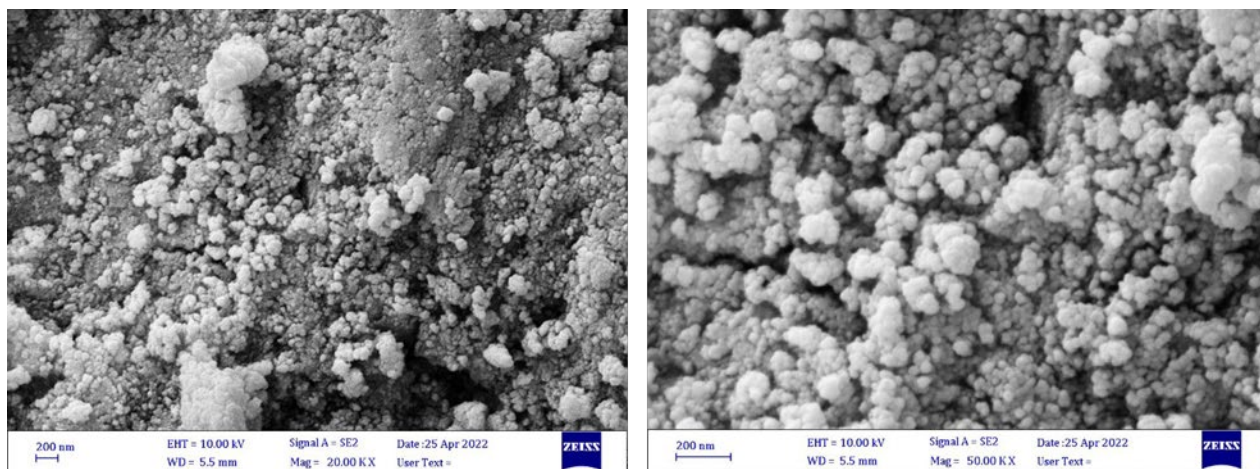
Figure 2. SEM Images of Cerium Oxide Nanoparticles

Transmission Electron Microscopy of CeO₂ Nanoparticles

TEM pictures of the sample were acquired and are displayed in Figure 3 to further the research of the morphology, as well as size, of the product as it was produced. The nanoparticle sizes determined by the XRD diffraction pattern and the TEM picture, which shows average sizes of 36 nm, are closely correlated. Understanding the crystalline characteristics of the nanoparticles is the aim of the TEM study
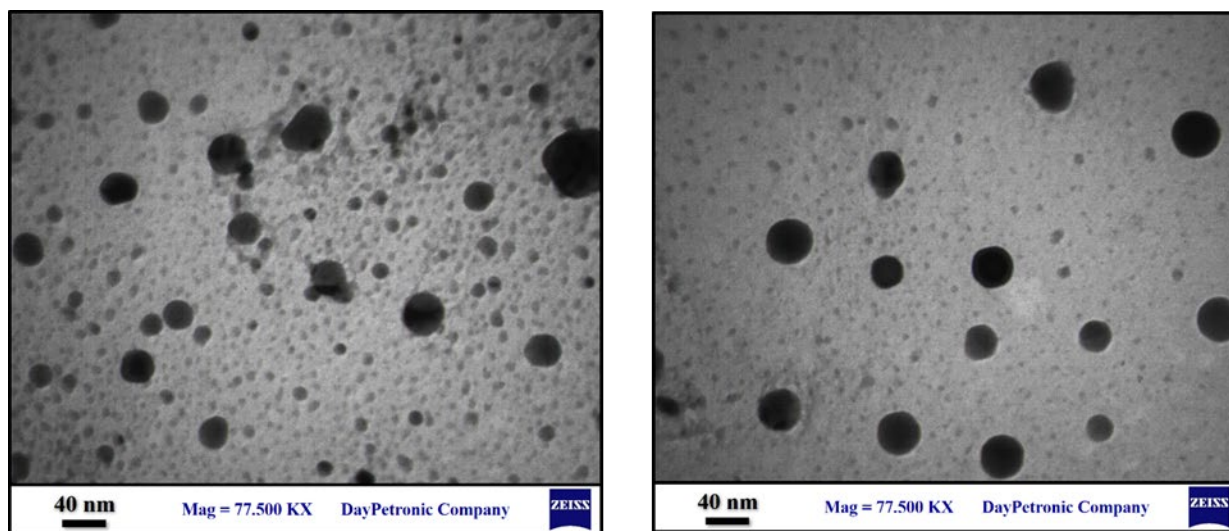

Figure 3. TEM Images of Cerium Oxide Nanoparticles

.

Characterization of Energy-dispersive X-ray Spectroscopes

The chemical composition and purity of the as-produced CeO₂ nanoparticles were examined using EDS analysis as shown in Figure 4.
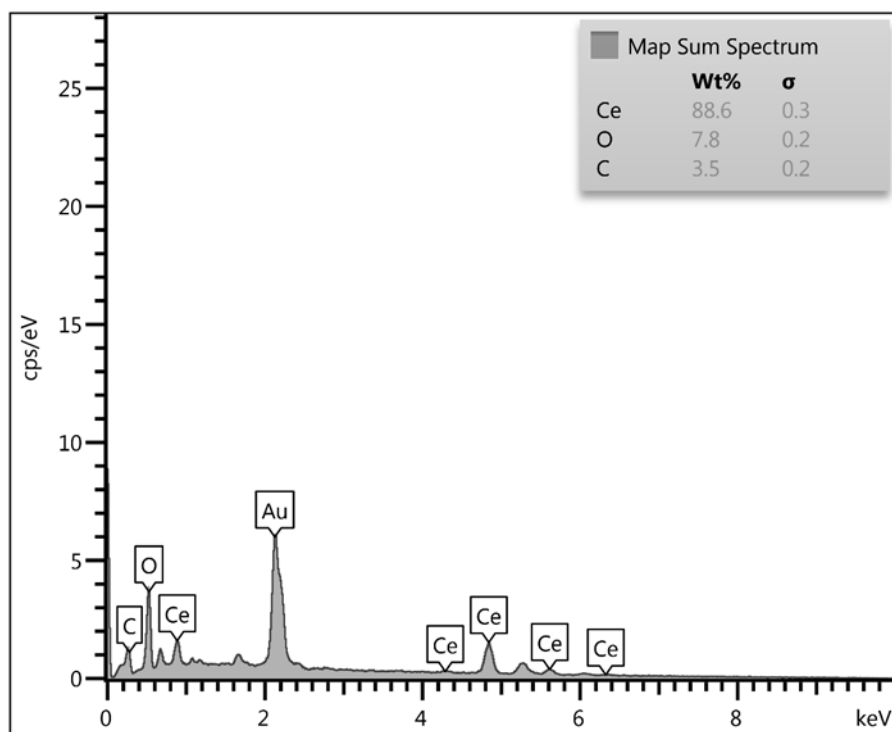
Figure 4. EDX Spectrum of Cerium Oxide Nanoparticles

The presence of Ce, as well as O, in the product is shown by a typical EDX spectrum, as seen in Figure 5. The silicon plates employed in the EDS instrument are what cause the presence of Si peaks in this spectrum.
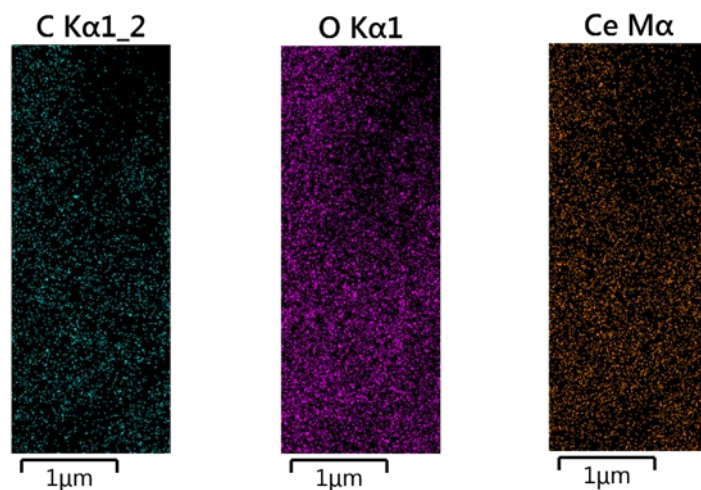

Figure 5. EDAX Mapping of Cerium Oxide Nanoparticles

Adsorption Isotherms

The major purpose of the adsorption analysis is to evaluate the correlation bet-ween the dye and adsorption by contrasting the adsorption isotherm with the adsorption data. This study evaluated both the Lang-muir and Freundlich models. The linear Freundlich adsorption process is represented by the following formula [10] [34-36]:

$$\log(Qe) = \log(kf) + \left(\frac{1}{n}\right) \log(Ce) \qquad (2)$$

The Freundlich constants, kf as well as n, respectively, show the adsorption capacity and intensity. As shown in Figure 6, while n is determined using the slope, kf is deter-mined using the intercept. In the cur-rent study, 1/n was found to be 0.5086 for the Freundlich CeO_2 isotherm. As a result, this research supported the value of physical adsorption. [37].
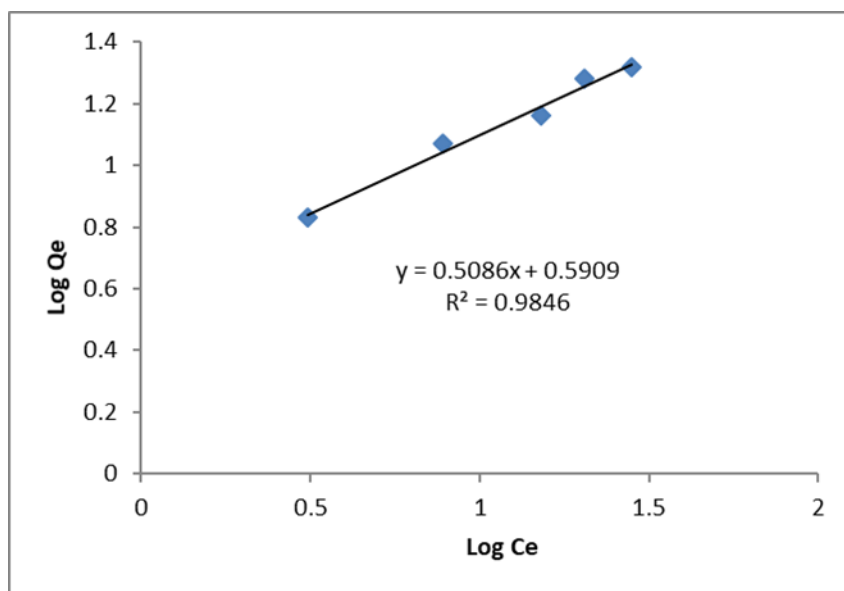

The plot shows data points with the fitted line:
$$y = 0.5086x + 0.5909$$
$$R^2 = 0.9846$$

with x-axis labeled "Log Ce" and y-axis labeled "Log Qe".

Figure 6. The Freundlich Isotherm Model Plot at 298 K

The Freundlich isotherm ($R^2 = 0.9846$) provides a better fit for the adsorption. The equation that follows shows how well the data fits the Langmuir adsorption isotherm [36,37]:

$$\frac{Ce}{Qe} = \frac{1}{q\,max}Kl + \frac{Ce}{q\,max} \qquad (3)$$

The Langmuir constant is Kl (mg/L), but the maximum adsorption of Cibacron red dye is q max (mg/g). The separation factor, often known as the dimensionless constant (Rl) [36], outlines and illustrates the main features of the Langmuir isotherm:

$$Rl = \frac{1}{(1 + Kl\ Ci)} \tag{4}$$

According to Figure 7, the dye adheres to CeO_2 the best when the initial dye concentration is Ci (mg/L) and the Rl values are all between (0-1).
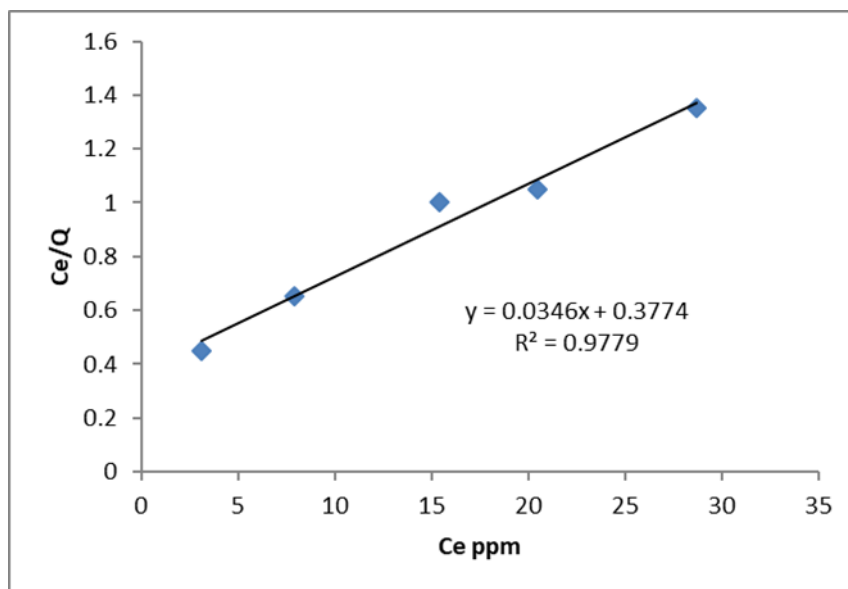

Figure 7. The Langmuir Isotherm Model at 298 K.

The graph shows Ce/Q versus Ce ppm with the equation y = 0.0346x + 0.3774 and R² = 0.9779.

The Effect of Contact Time

In series of experiments, 0.01 g CeO_2 nanoparticle and also 10 ml (50 ppm) dye were used to determine both contact time as well as equilibrium time. The liquid was warmed to 298 K with the use of a 200 rpm shaker. Adsorption happens rather quickly in the first 5 to 40 minutes. Due to the active CeO_2 nanoparticles' close association with the dye, quick adsorption is made feasible. After 35 minutes, the dye adsorption rate stabilizes due to the nanoparticles' surface, seen in Figure 8.
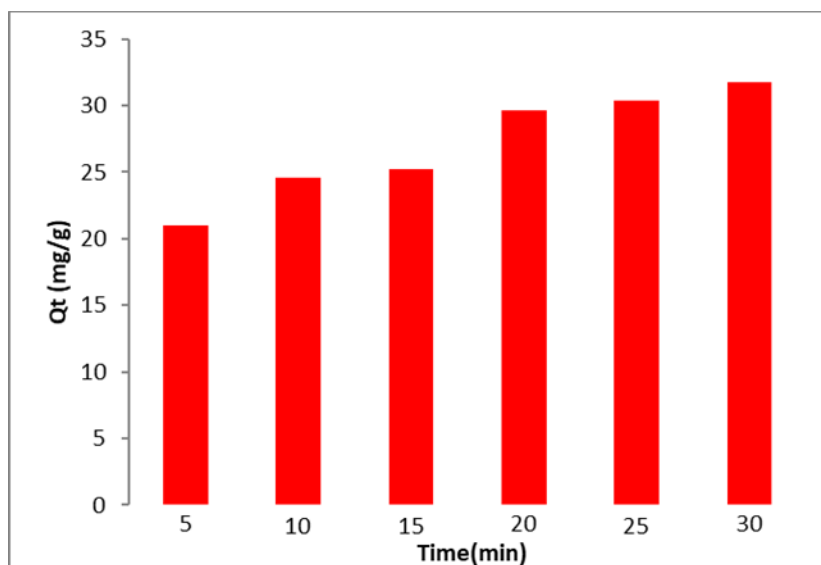
Figure 8. Effect of Time on Dye Adsorption onto the Cerium Oxide Nanoparticles

The Effect of Adsorbent Mass

Different masses of CeO_2 NPs (0.005g, 0.01g, 0.05g, 0.1g, and 0.15g) were added to 50 ppm of dye to evaluate the adsorbent's efficacy. The mixture was shaken at 298 K and 200 rpm. The graph illustrates the link between adsorption volume and mass. First, because nanoparticles have more active sites, adsorption occurs very quickly. Figure 9 shows how increasing the mass of the CeO_2 NPs led to an increase in dye ad-sorption.
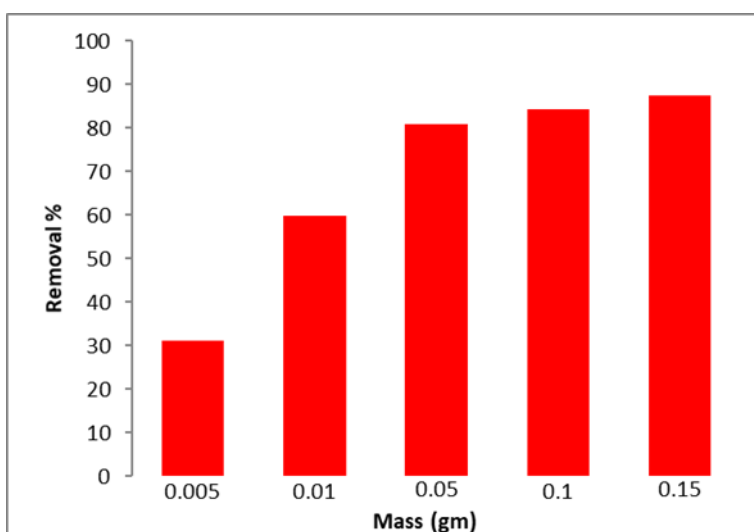

Figure 9. Effect of Adsorbent Mass on Adsorption of Dye onto the Cerium Oxide Nanoparticles

The Effect of Temperature

The effect of temperature on dye adsorption on the surface of CeO_2 NPs was investigated at a number of temperatures, including 288 K, 298 K, 308 K, 318 K, and 328 K. With rising temperature, the dye adsorption solution volume increases. As a result, the endothermic process occurs, and the average value of H° increases above zero. This clarifies how the absorption and adsorption processes work. As the temperature, the rate of diffusion accelerates, and a strong bond is established with the adsorbent, the diffusion molecules are absorbed by the holes. Since thermodynamic parameters provide exact information on changes in inherent energy brought on by adsorption, thorough evaluation of these parameters is crucial. The following adjustments were examined to estimate the adsorption process utilizing the free energy of adsorption ($\Delta G°$), entropy ($\Delta S°$), and also enthalpy ($\Delta H°$) [36-40]:

$$\ln(Ke) = \frac{-\Delta H}{RT} + \frac{\Delta S}{R} \tag{5}$$

$$Ke = \frac{Qe}{Ce} \tag{6}$$

$$\Delta G = \Delta H \_ T\Delta S \tag{7}$$

The equilibrium constant, Ke, the gas constant, and the temperature in Kelvin are all equal to 8.314 J/mol K (K). The interaction was endothermic, as shown by the Van 't Hoff plot in Figure 10 between ln K and 1/T, where the ΔH was 29.26 kJ/mole prevented by slope.
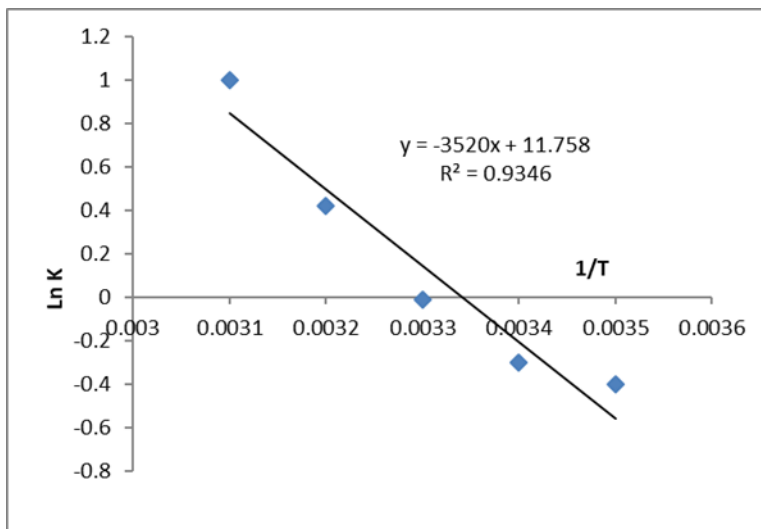

Figure 10. Van 't Hoff Plot Between Ln K and 1/T

The intercept's ΔS, which came out at 97.68 J/mole, showed that the adsorbed particles were still moving very near to the surface. They used the words "absorption" and "adsorption." The positive ΔG value at 293 K, which is 2.44 KJ/mol, points to non-spontaneous adsorption.

Dynamics

The kinetics of dye adsorption on the surface adsorbents of CeO_2 NPs determines the uses for adsorbents. The dye analysis revealed that the adsorption equilibrium duration for 0.01 g of the CeO_2 nanoparticle adsorbents was around 30 minutes. Additionally, the following data regarding adsorption was represented in this study using both classical and kinetic models:

Pseudo-first-order mathematical model [36–41]

$$\ln(qe - qt) = \ln(qe) - k1\,t \tag{8}$$

Figure 11 shows the pseudo-first-order rate constant, k1, the equilibrium adsorption capacity, qe (mg g^{-1}), and the amount of dye that has been adsorbed over time, qt (mg g^{-1}) (min^{-1}).
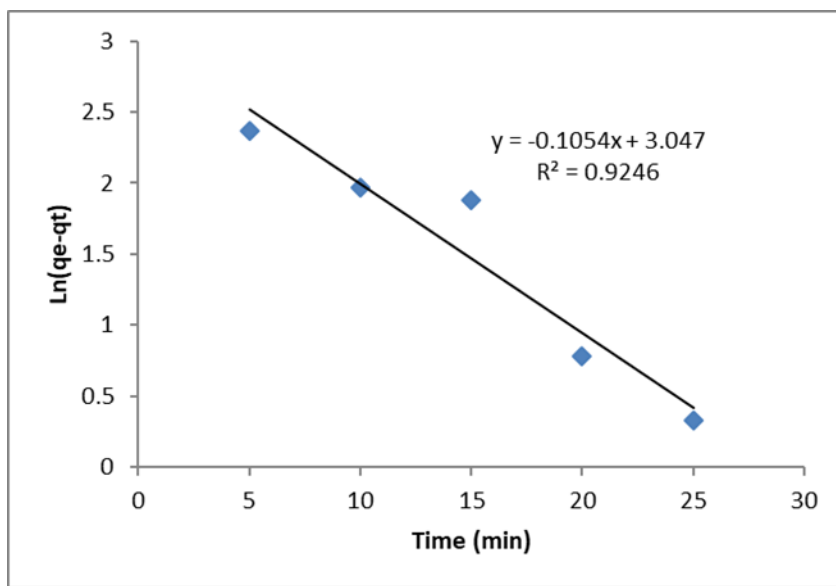

$$y = -0.1054x + 3.047$$
$$R^2 = 0.9246$$

Figure 11. Dynamic of Adsorption of Dye Pseudo-first-order

The pseudo-second-order kinetic model is as follows, as seen in [10-12]:

$$\frac{1}{qt} = \frac{1}{k2\,qe} + \frac{t}{qe} \tag{9}$$

The hypothetical second-order rate constant is denoted by K2.

The pseudo-second-order model with a strong association factor ($R^2 > 0.9873$) may adequately capture the kinetic information, as shown in Figure 12.
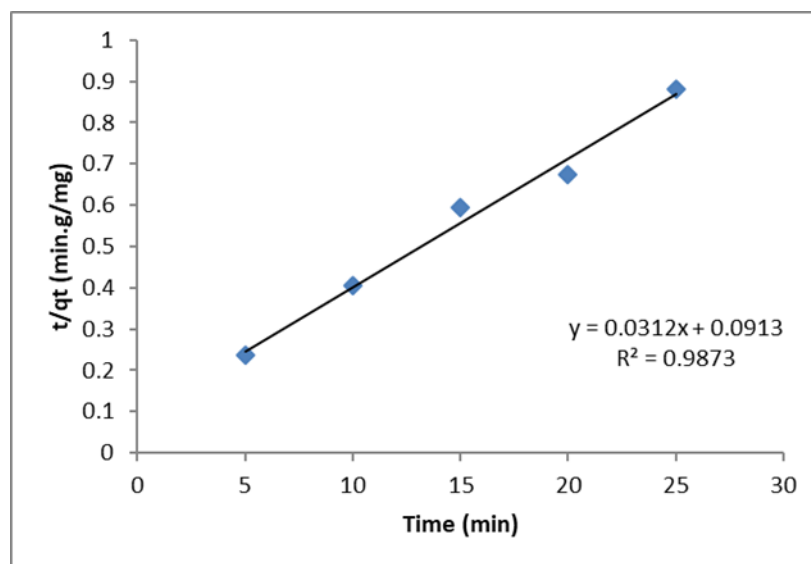

Figure 12. Dynamic of Adsorption of Dye Pseudo-second-order

4. Conclusion

Green synthesis was used to create high-quality CeO_2, and XRD, SEM/EDX, and TEM images were taken. The CeO_2 NPs' particle sizes varied, according to TEM analysis, and ranged from 28-36 nm. The observed adsorption properties are perfect for removing dye from aqueous solutions. In both kinetic and thermodynamic experiments, CeO_2 NPs proved to be effective as adsorbers. The outcomes fit the Langmuir and Freundlich isotherm models rather well.

The adsorption is much better captured by the Freundlich isotherm model. The adsorption is endothermic and spontaneous, as per thermodynamics. The slope of the Van 't Hoff plot was used to calculate the enthalpy value, which describes the physical characteristics of the adsorption and is equal to 29.26 kJ/mole. With an R^2 value of 0.9873, this adsorption complies with pseudo-second-order.

5. References

1. Shen F, Zhang L, Jiang L, Tang M, Gai X, Chen M, Ge X. Temporal variations of six ambient criteria air pollutants from 2015 to 2018, their spatial distributions, health risks and relationships with socioeconomic factors during 2018 in China. *Environ. Int.*, 2020, 137, 105556.
2. Kamil AF, Abdullah HI, Mohammed SH. Cibacron red dye removal in aqueous solution using synthesized $CuNiFe_2O_5$ Nanocomposite: thermodynamic

and kinetic studies. *Egypt. J. Chem.*, 2021, 64(11), 5-6.

3. Wang X, Chen Y, Li Z, Fang G, Wang Y. Development and utilization of water resources and assessment of water security in Central Asia. *Agric. Water Manage.*, 2020, 240, 106297.

4. Muthukrishnan L. Nanotechnology for cleaner leather production: A review. *Environ. Chem. Lett.*, 2021, 1-23.

5. Chowdhary P, Bharagava RN, Mishra S, Khan N in Environmental Concerns and Sustainable Development, Springer, Singapore, 2020, Role of Industries in Water Scarcity and Its Adverse Effects on Environment and Human Health, pp 235-256.

6. Lesimple A, Jasim SY, Johnson DJ, Hilal N. The role of wastewater treatment plants as tools for SARS-CoV-2 early detection and removal. *J. Water Process Eng.*, 2020, 101544.

7. Saleh IA, Zouari N, Al-Ghouti MA. Removal of pesticides from water and wastewater: Chemical, physical and biological treatment approaches. *Environ. Technol. Innovation*, 2020, 101026.

8. Shah I, Adnan RA. Comprehensive review on the hierarchical performances of eco-friendly and functionally advanced modified and recyclable carbon materials. *J. Iran. Chem. Soc.*, 2020, 17(7), 1521-1537.

9. Heidarinejad Z, Dehghani MH, Heidari M, Javedan G, Ali I, Sillanpää M. Methods for preparation and activation of activated carbon: A review. *Environ. Chem. Lett.*, 2020, 18(2), 393-415.

10. Rheima AM, Mahmood RS, Hussain DH, Abbas ZS. Study the adsorption ability of alizarin red dye from their aqueous solution on synthesized carbon nanotubes. *Dig. J. Nanomater. Biostructures*, 2020, 15(4).

11. Nguyen CH, Tran HN, Fu CC, Lu YT, Juang RS. Roles of adsorption and photocatalysis in removing organic pollutants from water by activated carbon-supported titania composites: Kinetic aspects. *J. Taiwan Inst. Chem. Eng.*, 2020, 109, 51-61.

12. Zhang H, Nengzi LC, Wang Z, Zhang X, Li B, Cheng X. Construction of Bi_2O_3/CuNiFe LDHs composite and its enhanced photocatalytic degradation of lomefloxacin with persulfate under simulated sunlight. *J. Hazard. Mater.*, 2020, 383, 121236.

13. Abdulah HI, Rheima AM, Hussain DH, Abed HJ. Synthesis of Fe_2O_3 nanoparticles by photolysis method for novel dye-sensitized solar cell. *J. Adv. Sci. Nanotechnol.*, 2022, 1(1), 1-8.

14. Al-Uqaily RA, Rheima AM, Jaber SH, Mohammed SH, Abbas ZS, Abjel AK, Falih SS in AIP Conference Proceedings, AIP Publishing LLC, 2022, vol. 2450, no. 1, Nano-metal Complex Inhibitor for Mild Steel Corrosion in Acidic Media: A Comparative Study on Inhibitor Concentrations, p 020047.

15. Rheima AM, Anber AA, Abdullah HI, Ismail AH. Synthesis of alpha-gamma aluminum oxide nanocomposite via electrochemical method for antibacterial activity. *Nano Biomed. Eng.*, 2021, 13(1), 1-5.

16. Al Marjani M, Aziz SN, Rheima AM, Abbas ZS. Impact of chromium oxide nanoparticles on growth and biofilm formation of persistence Klebsiella pneumoniae isolates. *Nano Biomed. Eng.*, 2021, 13(3), 321-327.

17. Kadhum HA, Salih WM, Rheima AM. Improved PSi/c-Si and Ga/PSi/c-Si nanostructures dependent solar cell efficiency. *Appl. Phys. A*, 2020, 126(10), 1-5.

18. Aboud NAA, Alkayat WM, Hussain DH, Rheima AM in Journal of Physics: Conference Series, IOP Publishing, 2020, vol. 1664, no. 1, A Comparative Study of ZnO, CuO and a Binary Mixture of ZnO 0.5-CuO 0.5 with Nano-dye on the Efficiency of the Dye-sensitized Solar Cell, p 012094.

19. Aziz SN, Al Marjani MF, Rheima AM, Al Kadmy IM. Antibacterial, antibiofilm, and antipersister cells formation of green synthesis silver nanoparticles and graphene nanosheets against Klebsiella pneumoniae. *Rev. Med. Microbiol.*, 2022, 33(1), 56-63.

20. Salman AT, Ismail AH, Rheima AM, Abd AN, Habubi NF, Abbas ZS in Journal of Physics: Conference Series, IOP Publishing, 2021, vol. 1853, no. 1, Nano-synthesis, Characterization and Spectroscopic Studies of Chromium (III) Complex Derived from New Quinoline-2-one for Solar Cell Fabrication, p 012021.

21. Ismail AH, Al-Bairmani HK, Abbas ZS, Rheima AM in IOP Conference Series: Materials Science and Engineering, IOP Publishing, 2020, vol. 928, no. 5, Nano Metal-complexes of Theophylline Derivative: Synthesis, Characterization, Molecular Structure Studies, and Antibacterial Activity, p 052028.

22. Kamil AF, Abdullah H, Rheima AM, Mohammed SH. Photochemical synthesized NiO nanoparticles based dye-sensitized solar cells: a comparative study on the counter electrodes and dye-sensitized concentrations. *J. Ovonic Res.*, 2021, 17(3), 299-305.

23. Mohammed SH, Rheima A, Al-Jaafari F, Al-Marjani, MF. Green-synthesis of platinum nanoparticles using olive leaves extracts and its effect on aspartate aminotransferase activity. *Egypt. J. Chem.*, 202265(4), 1-2.

24. Ismail AH, Al-Bairmani HK, Abbas ZS, Rheima AM. Nanosynthesis, spectroscopic characterisation and antibacterial activity of some metal complexes derived from Theophylline. *Egypt. J. Chem.*, 2020, 63(12), 4951-4962.

25. Trovarelli A, Zamar F, Llorca J, de Leitenburg C, Dolcetti G, Kiss JT. *J. Catal.*, 1997, 169, 490-502.

26. Steele BCH. Mass transport in materials incorporated in electrochemical energy conversion systems. *Solid State Ionics*, 1984, 12, 391-406.

27. Mogensen M, Sammes NM, Tompsett GA. Physical, chemical and electrochemical properties of pure and doped ceria. *Solid State Ionics*, 2000, 129(1-4), 63-94.

28. Zhang F, Chan SW, Spanier JE, Apak E, Jin Q, Robinson RD, Herman IP. Cerium oxide nanoparticles: Size-selective formation and structure analysis. *Appl. Phys. Lett.*, 2002, 80(1), 127-129.

29. Tye L, El-Masry NA, Chikyow T, McLarty P, Bedair SM. Electrical characteristics of epitaxial CeO$_2$ on Si (111). *Appl. Phys. Lett.*, 1994, 65(24), 3081-3083.

30. Ali MM, Mahdi HS, Parveen A, Azam A in AIP Conference Proceedings, AIP Publishing LLC, 2018, vol. 1953, no. 1, Optical Properties of Cerium Oxide (CeO2) Nanoparticles Synthesized by Hydroxide Mediated Method, p 030044.

31. Xia T, Kovochich M, Liong M, Madler L, Gilbert B, Shi H, Yeh JI, Zink JI, Nel, AE. Comparison of the mechanism of toxicity of zinc oxide and cerium oxide nanoparticles based on dissolution and oxidative stress properties. *ACS Nano*, 2008, 2(10), 2121-2134.

32. Tarnuzzer RW, Colon J, Patil S, Seal S. Vacancy engineered ceria nanostructures for protection from radiation-induced cellular damage. *Nano Lett.*, 2005, 5(12), 2573-2577.

33. Chelliah M, Rayappan JBB, Krishnan UM. Synthesis and characterization of cerium oxide nanoparticles by hydroxide mediated approach. *J. Appl. Sci.*, 2012, 12(16), 1734-1737.

34. Rheima A, Anber AA, Shakir A, Salah Hammed A, Hameed S. Novel method to synthesis nickel oxide nanoparticles for antibacterial activity. *Iran. J. Phys. Res.*, 2020, 20(3), 51-55.

35. Mohammed MA, Rheima AM, Jaber SH, Hameed SA. The removal of zinc ions from their aqueous solutions by Cr$_2$O$_3$ nanoparticles synthesized via the UV-irradiation method. *Egypt. J. Chem.*, 2020, 63(2), 425-431.

36. Rheima AM, Mohammed MA, Jaber SH, Hameed SA. Adsorption of selenium (Se^{4+}) ions pollution by pure rutile titanium dioxide nanosheets electrochemically synthesized. *Desalin. Water Treat.*, 2020, 194, 187-193.

37. Aboud NAA, Jasim BE, Rheima AM. Methylene orange dye removal in aqueous solution using synthesized CdO-MnO2 nanocomposite: Kinetic and thermodynamic studies. *Chalcogenide Lett.*, 2021, 18(5), 237-243.

38. Hussain DH, Rheima AM, Jaber SH. Cadmium ions pollution treatments in aqueous solution using electrochemically synthesized gamma aluminum oxide nanoparticles with DFT study. *Egypt. J. Chem.*, 2020, 63(2), 417-424.

39. Rheima AM, Hussain DH, Almijbilee, MMA. Graphene-silver nanocomposite: synthesis, and adsorption study of cibacron blue dye from their aqueous solution. *J. Southwest Jiaotong Univ.*, 2019, 54(6).

40. Satilmis B. Amidoxime modified polymers of intrinsic microporosity (PIM-1); A versatile adsorbent for efficient removal of charged dyes; Equilibrium, kinetic and thermodynamic studies. *J. Polym. Environ.*, 2020, 28(3), 995-1009.

41. Ezzati R. Derivation of pseudo-first-order, pseudo-second-order and modified pseudo-first-order rate equations from Langmuir and Freundlich isotherms for adsorption. *Chem. Eng. J.*, 2020, 392, 123705.